

DeflareMamba: Hierarchical Vision Mamba for Contextually Consistent Lens Flare Removal

Yihang Huang

School of Artificial Intelligence, Beijing Normal University
Beijing, China

Yuanfei Huang*

School of Artificial Intelligence, Beijing Normal University
Engineering Research Center of Intelligent Technology
and Educational Application, Ministry of Education
Beijing, China

Junhui Lin

School of Artificial Intelligence, Beijing Normal University
Beijing, China

Hua Huang

School of Artificial Intelligence, Beijing Normal University
Engineering Research Center of Intelligent Technology
and Educational Application, Ministry of Education
Beijing, China

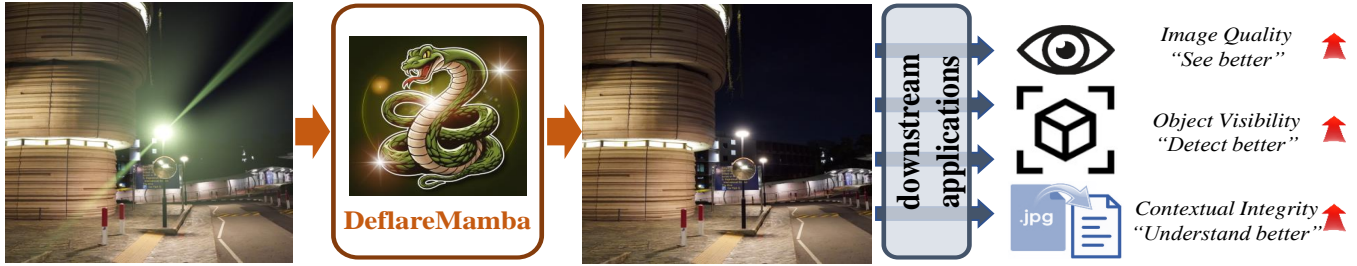


Figure 1: DeflareMamba effectively enhances the quality of image media, thereby enabling downstream applications that benefit from improved image quality, increased object visibility, and enhanced contextual integrity.

ABSTRACT

Lens flare removal remains an information confusion challenge in the underlying image background and the optical flares, due to the complex optical interactions between light sources and camera lens. While recent solutions have shown promise in decoupling the flare corruption from image, they often fail to maintain contextual consistency, leading to incomplete and inconsistent flare removal. To eliminate this limitation, we propose DeflareMamba, which leverages the efficient sequence modeling capabilities of state space models while maintains the ability to capture local-global dependencies. Particularly, we design a hierarchical framework that establishes long-range pixel correlations through varied stride sampling patterns, and utilize local-enhanced state space models that simultaneously preserves local details. To the best of our knowledge, this is the first work that introduces state space models to the flare removal task. Extensive experiments demonstrate that our

method effectively removes various types of flare artifacts, including scattering and reflective flares, while maintaining the natural appearance of non-flare regions. Further downstream applications demonstrate the capacity of our method to improve visual object recognition and cross-modal semantic understanding. Code is available at <https://github.com/BNU-ERC-ITEA/DeflareMamba>.

CCS CONCEPTS

• Computing methodologies → Image processing.

KEYWORDS

Lens flare removal, Mamba, contextual consistency

ACM Reference Format:

Yihang Huang, Yuanfei Huang, Junhui Lin, and Hua Huang. 2025. DeflareMamba: Hierarchical Vision Mamba for Contextually Consistent Lens Flare Removal. In *Proceedings of the 33rd ACM International Conference on Multimedia (MM '25)*, October 27–31, 2025, Dublin, Ireland. ACM, New York, NY, USA, 10 pages. <https://doi.org/10.1145/3746027.3755263>

1 INTRODUCTION

Lens flare [12, 19, 30] fundamentally represents a parasitic signal that nonlinearly couples with the intrinsic image content. This coupling leads to significant degradation in the quality of images and videos. Firstly, it severely compromises the visual quality and deteriorates user experience by introducing undesired artifacts, e.g., irregular luminance patterns and color shifts. Besides, these artifacts can also degrade the performance of downstream vision tasks like

*Corresponding author. Email: yfhuang@bnu.edu.cn

Permission to make digital or hard copies of all or part of this work for personal or classroom use is granted without fee provided that copies are not made or distributed for profit or commercial advantage and that copies bear this notice and the full citation on the first page. Copyrights for components of this work owned by others than the author(s) must be honored. Abstracting with credit is permitted. To copy otherwise, or republish, to post on servers or to redistribute to lists, requires prior specific permission and/or a fee. Request permissions from [permissions@acm.org](https://permissions.acm.org).

MM '25, October 27–31, 2025, Dublin, Ireland

© 2025 Copyright held by the owner/author(s). Publication rights licensed to ACM.
ACM ISBN 979-8-4007-2035-2/2025/10...\$15.00
<https://doi.org/10.1145/3746027.3755263>

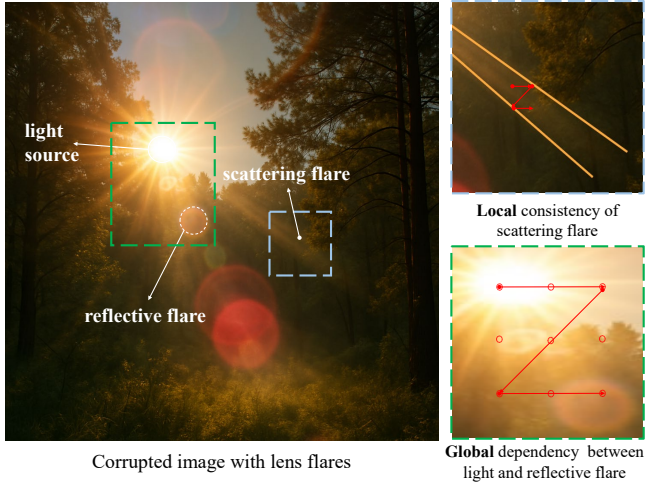


Figure 2: Global-local contextual consistency of lens flares. Exploring global-local scanning strategy is an intuitive solution to model the structure of flares and remove them.

object detection and recognition. Moreover, in cross-modal tasks, such as image-text or video-audio alignment, these artifacts may introduce semantic noise that disrupts the correspondence between modalities. In Figure 1, it is crucial to decoupling these optical artifacts from the intrinsic scene information, thereby ensuring clean input data for multimedia and multimodal applications [27].

Lens flare manifests primarily in two forms: scattering flare and reflective flare[16]. Scattering flare originates from the interaction between light and microscopic imperfections in the lens, resulting in diffuse streak effects. In contrast, reflective flare arises from internal reflections between lens elements, producing distinctive geometric shapes such as concentric rings or polygons. These artifacts are further amplified in low-light conditions, where the interaction between strong light sources and camera optics produces more pronounced and intricate flare patterns that weaken visual features.

In Figure 2, maintaining contextual consistency is crucial for flare removal tasks. It ensures that the restored image preserves semantic coherence of the original scene content. Specifically, scattering flare, characterized by localized light diffusion patterns around strong light sources, necessitates local contextual consistency to seamlessly blend the affected regions with their surroundings in terms of color saturation, texture fidelity, and edge sharpness. In contrast, reflective flare originates from the light source and produces secondary bright spots through lens reflections. These flares maintain specific spatial relationships with their corresponding light sources. Thus, their removal requires coordinated processing of both the flare patterns and the associated light sources, emphasizing global semantic consistency to capture and restore the long-range relationships between light source and the induced flare patterns. In this way, global semantic consistency facilitates detail preservation while maintaining overall scene integrity.

However, existing deep learning architectures face significant challenges in maintaining such contextual consistency. CNN-based approaches [13, 26, 31] are limited by their local receptive fields,

making them inadequate for modeling long-range dependencies. Although Transformer-based methods [38, 41] offer enhanced global context modeling, their quadratic computational complexity restricts the processing of high-resolution images. While windowed self-attention mechanisms [25] attempt to mitigate this limitation, they often compromise the ability to capture the global dependencies essential for effective flare removal.

Recently, the Mamba architecture [8] has emerged as a promising alternative for sequence modeling. It employs State Space Models (SSMs) with data-dependent parameters, enabling efficient sequence processing with linear computational complexity. Adapting Mamba for vision tasks requires selective scan mechanisms that transform 2D image data into 1D sequences for processing. Through this mechanism, pioneering works such as ViM [48] and VMamba [24] have achieved comparable or superior performance to state-of-the-art architectures across various vision tasks. Furthermore, MambaIR [10] demonstrates Mamba’s effectiveness in image restoration, achieving remarkable results in super-resolution, denoising, and other enhancement tasks.

Nevertheless, MambaIR encounters significant challenges in maintaining contextual consistency due to two primary issues:

1) Conventional selective scan in SSMs prioritizes broader patterns at the expense of fine-grained details, thereby overlooking the intricate relationships among local neighboring pixels. This lack of localized modeling undermines the capture of contextual dependencies critical for restoring subtle transitions and ensuring coherence within affected regions.

2) SSMs exhibit a long-term decay property, where the correlation between sequential elements diminishes as their distance increases. As illustrated in Figure 2, conventional selective scan strategies may map spatially adjacent flare-affected pixels to distant positions in the sequence domain. This spatial inconsistency is particularly problematic for reflective flares which often appear far from their light sources. Such spatial inconsistency prevents the effective capture of both local details and global patterns essential for high-quality flare removal.

To address these challenges, we propose DeflareMamba, an SSM-based model specifically designed for flare removal. Our approach focuses on preserving both local spatial coherence and global structural integrity through innovative scanning strategies. Our contributions are summarized as follows:

- To the best of our knowledge, this is the first work to apply Mamba for flare removal. Our experiments demonstrate that contextually consistent Mamba models can effectively address flare removal challenges, achieving promising results.
- We propose a novel hierarchical framework to simultaneously capture both local spatial coherence and global structural integrity, ensuring contextual coherence across multiple spatial scales, especially critical for handling complex flare patterns spanning various regions of the image.
- We utilize a Local-enhanced Selective Scan mechanism that effectively maintains contextual consistency between flare-affected regions and surroundings. It is specifically designed to address the inherent limitations of conventional scanning approaches in preserving spatial relationships between light sources and their associated flare artifacts.

Extensive experiments on benchmark datasets demonstrate that DeflareMamba outperforms state-of-the-art methods in both quantitative metrics and visual quality. Furthermore, several downstream applications highlight the superiority of our method in improving both single-modal and cross-modal understanding.

2 RELATED WORK

2.1 Flare Removal

Early methods for flare removal adopted a detection-based strategy [1, 2, 36], wherein flare regions are first identified based on their visual features, and subsequent restoration algorithms [3] are employed to remove the flares. However, these methods suffer from two primary drawbacks: they are effective only for specific flare types, and they often mistake bright objects in the image for flare artifacts. Recent advances in data-driven approaches have considerably enhanced flare removal performance, with several innovative methods addressing the challenges associated with training data generation. Wu et al. [39] introduced a synthesis framework that leverages light source guidance for single-image flare removal. A significant breakthrough occurred with Dai et al. [4], who introduced the Flare7K dataset as the first comprehensive benchmark for nighttime flare removal research. This dataset has spurred several follow-up studies [34, 43, 47] that have further advanced flare removal techniques. Subsequently, they extended this work with Flare7K++ [5], which incorporates real-world flare data and proposes an enhanced removal pipeline, thereby achieving substantial improvements in performance.

Currently, there are only three publicly available datasets for flare removal: the dataset proposed by Wu et al. [39], Flare7K [4], and Flare7K++ [5]. While Wu's dataset only provides evaluation results on U-Net and their proposed network, the Flare7K++ dataset encompasses Flare7K and offers comprehensive benchmarking results across multiple state-of-the-art models. Therefore, we adopt Flare7K++ as our primary dataset for both training and evaluation.

2.2 Image Restoration with Vision Mamba

CNN-based or Transformer-based methods The evolution of image restoration techniques has witnessed a paradigm shift from traditional methods to deep learning approaches. CNN-based methods [6, 17, 22, 42, 45] have demonstrated significant advantages over traditional approaches, offering faster training, automatic feature extraction, and superior restoration quality. However, these methods are inherently limited by their local receptive fields, constraining their ability to capture long-range dependencies. Transformer-based architectures [21, 38, 41] emerged as a promising solution, introducing self-attention mechanisms that excel at modeling global relationships in images. While these methods achieve impressive restoration results through their ability to capture long-range dependencies, they face challenges in computational efficiency, particularly when processing high-resolution images due to the quadratic complexity of self-attention operations. This limitation often necessitates the use of local-window self-attention mechanisms, resulting in an inevitable trade-off between global receptive field and computational cost.

Vision Mamba The Mamba architecture, based on state space models, introduces an innovative selective state update mechanism

that enables efficient modeling of long-range dependencies while maintaining linear computational complexity. A critical challenge in applying the Mamba architecture to image restoration lies in the design of selective scan strategies that transform 2D images into 1D sequences amenable to processing by SSMs. While early approaches, such as VIM, utilized simple row-wise scanning to convert 2D features into 1D sequences, this method risked discarding critical spatial structural information inherent in the multi-dimensional nature of images (i.e., height, width, and channels). To overcome this limitation, several innovative scanning strategies have been proposed: VMamba introduced bidirectional scanning; LocalMamba [11] developed a local scanning mechanism through image partitioning, PlainMamba [40] implemented Z-pattern scanning to preserve spatial continuity, and EfficientVMamba [28] proposed interval scanning with sub-image sampling to enhance computational efficiency. Despite these advancements, preserving fine details and maintaining global structural integrity in image restoration remains an active area of research.

3 PRELIMINARIES

3.1 State Space Models

State Space Models (SSMs) [9][8] have gained attention for their ability to model long-range dependencies with linear computational complexity relative to the input length. A continuous-time linear SSM can be described as:

$$\frac{d}{dt}h(t) = Ah(t) + Bx(t), \quad y(t) = Ch(t) + Dx(t), \quad (1)$$

where $h(t) \in \mathbb{R}^N$ is the hidden state, $x(t)$ is the input, $y(t)$ is the output, and A, B, C, D are learnable matrices that define the system dynamics.

For practical use in deep learning, SSMs are discretized using techniques like Zero-Order Hold (ZOH)[8], resulting in:

$$h_k = \bar{A}h_{k-1} + \bar{B}x_k, \quad y_k = Ch_k + Dx_k, \quad (2)$$

with the discretized matrices given by:

$$\bar{A} = e^{\Delta A}, \quad \bar{B} = (\Delta A)^{-1}(e^{\Delta A} - I)B, \quad (3)$$

where Δ is the step size used in discretization.

The discrete form enables efficient parallelization using convolution:

$$y = x \otimes K, \quad K = (C\bar{B}, C\bar{A}\bar{B}, \dots, C\bar{A}^{L-1}\bar{B}), \quad (4)$$

where \otimes denotes convolution. This formulation allows fast inference and training, making SSMs suitable for high-resolution image restoration tasks, including flare removal.

3.2 Long-Term Decay Property of SSM

Despite their efficiency, standard SSMs suffer from a key limitation[32]: the long-term decay property. This issue causes the influence of earlier tokens in a sequence to diminish quickly over time, leading to long-range information loss. Formally, the contribution of a past token m to a future token n ($m < n$) is computed as:

$$C_n \prod_{i=m}^n \bar{A}_i \bar{B}_m = C_n \bar{A}_{(m \rightarrow n)} \bar{B}_m, \quad (5)$$

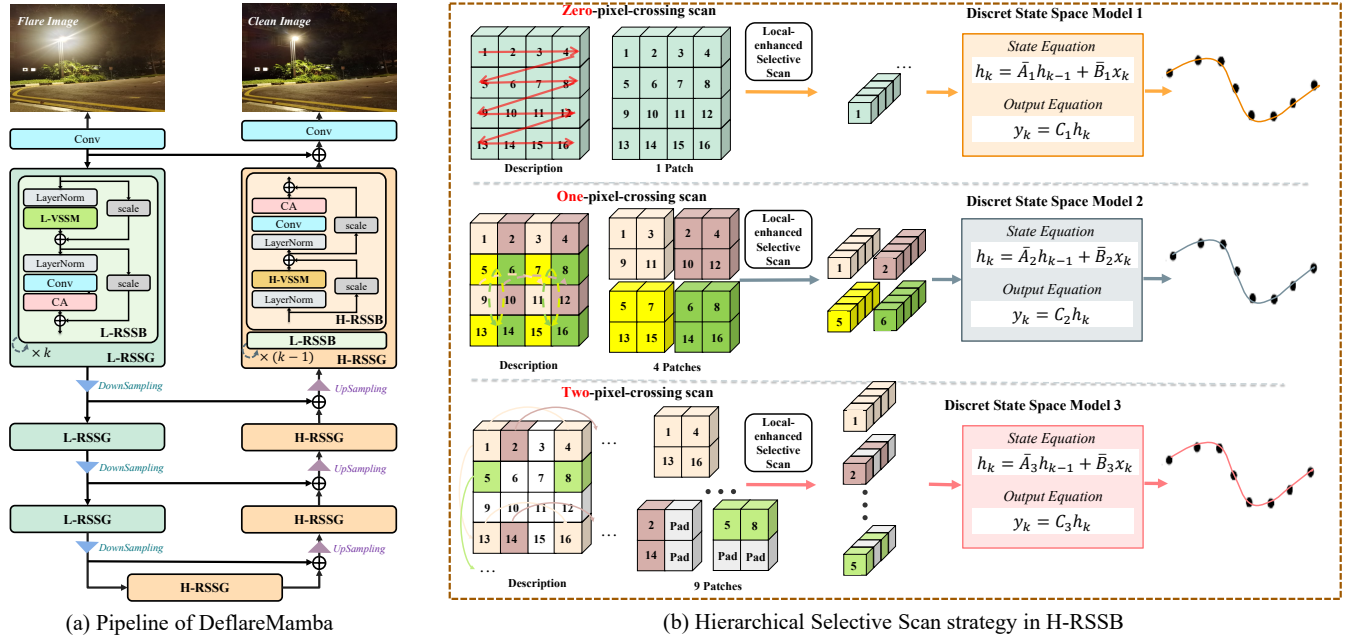


Figure 3: Overview of our DeflareMamba framework. The network adopts a U-shaped architecture with Local-enhanced Residue State Space Groups in the encoding stage and Hierarchical Residue State Space Groups in the decoding stage.

where

$$\bar{A}_{(m \rightarrow n)} = e^{\sum_{i=m}^n \Delta_i A}. \quad (6)$$

Since the learned $\Delta_i A$ values are typically negative [32], the exponential term $e^{\sum_{i=m}^n \Delta_i A}$ decays rapidly as the distance $(n - m)$ increases. As a result, the effect of earlier inputs fades quickly, limiting the model’s ability to retain long-range contextual information—an important factor in image restoration tasks that involve large and spatially dispersed artifacts.

Besides, most discrete SSMs are inherently causal. Their representations are unidirectional, with information flowing only from earlier to later tokens. This design restricts later tokens from contributing to the representations of earlier ones, making it difficult to model bidirectional dependencies or global interactions effectively. These two limitations—the long-term decay and causal structure—pose challenges for flare removal, where maintaining semantic consistency across distant and structurally connected regions is essential. Addressing these limitations is crucial for developing more capable architectures for image restoration.

4 METHOD

4.1 Overall Architecture

Our DeflareMamba framework employs a U-shaped[31] network architecture composed of several Local-enhanced and Hierarchical Residue State Space Groups (L-RSSG and H-RSSG), as illustrated in Figure 3. In this section, we first introduce the overall U-shaped network structure and detail the composition of L/H-RSSG. Then, we elaborate on the key enhancement mechanisms in our architecture: the Local-enhanced SSM in L-RSSG, which maintains local contextual consistency; and finally, the innovative Hierarchical

Selective Scan mechanism in H-RSSG, which establishes global semantic consistency essential for effective flare pattern recognition and removal.

U-shaped architecture. The input resolution required for flare removal tasks is typically 512×512 , which is substantially larger than the patch size processed in MambaIR[10]. Due to the long-term decay property of SSM, the correlation between pixels weakens as their sequence distance increases. The U-shaped structure can address this limitation through two key aspects. First, downsampling operations aggregate information from surrounding pixels, enlarging the receptive field of each element in the SSM sequence. Second, reduced resolution shortens sequence lengths, enhancing correlation between distant pixels in the original image.

Therefore, we adopt a U-shaped network architecture that specifically targets the unique requirements of flare removal. Specifically, given an input image $I \in \mathbb{R}^{H \times W \times 3}$, we first perform coarse feature extraction through a convolutional layer to project the image into a higher-dimensional embedding space $\mathbb{R}^{H \times W \times C}$. The extracted feature maps are subsequently processed by a U-shaped network architecture that comprises an encoding stage and a decoding stage.

1) In the encoding stage, we employ Local-enhanced Residue State Space Groups (L-RSSG) for hierarchical feature extraction. Within the l -th L-RSSG, features first pass through l consecutive Local-enhanced Residue State Space Blocks (L-RSSB) for deep feature extraction. Each L-RSSB is designed to capture fine-grained local details. An additional convolutional layer is introduced at the end of each group to refine the extracted features, followed by an element-wise summation with the input through a residual connection to facilitate gradient flow and prevent feature degradation during deep propagation.

2) In the decoding stage, we adopt Hierarchical Residue State Space Groups (H-RSSG) to process features at different scales. The structure of H-RSSG closely mirrors that of L-RSSG, beginning with $l - 1$ L-RSSB blocks and concluding with a convolutional layer and residual connection. The key distinction lies in the final block, where we replace the standard L-RSSB with our Hierarchical RSSB (H-RSSB) to enable comprehensive hierarchical feature extraction. This novel H-RSSB incorporates varied stride sampling patterns to establish long-range pixel correlations, effectively capturing both local details and global structural information necessary for high-quality flare removal.

Following the pipeline established in Flare7k++[5], the output features from our U-shaped network are projected through a convolutional layer to produce a 6-channel output tensor $O \in \mathbb{R}^{H \times W \times 6}$. The first three channels $O_{1:3}$ represent the flare-free image, serving as the primary output for the flare removal task, while the remaining three channels $O_{4:6}$ contain the predicted flare image, which is utilized in computing auxiliary losses to facilitate better network optimization.

Local-enhanced/Hierarchical Residue State Space Blocks. The basic blocks L-RSSB and H-RSSB in our architecture follow the structure of RSSB proposed in MambaR [2], but incorporate our improved selective scan mechanism to enhance the model’s capability in capturing global-local context consistency. Similar to the Transformer architecture’s flow of Norm \rightarrow Attention \rightarrow Norm \rightarrow MLP, our H/L-RSSB replaces the self-attention mechanism with our proposed H/L-VSSM (Hierarchical/Local-enhanced Vision State Space Module).

Given an input feature map $X \in \mathbb{R}^{H \times W \times C}$, the H/L-VSSM first applies layer normalization:

$$X_1 = LN(X), \quad (7)$$

As shown in Figure 3, the normalized features are then processed through two parallel branches. The main branch incorporates a depth-wise convolution (DWConv) for local feature extraction, followed by our improved two-dimensional state space model Ψ_{SSM} :

$$X_m = \Phi_1(\Psi_{SSM}(\sigma(DWConv(X_1)))), \quad (8)$$

where Ψ_{SSM} represents either the Local-Enhanced SSM (L-SSM) in the encoder path or Hierarchical SSM (M-SSM) in the decoder path, as illustrated in the detailed block diagrams. The skip branch applies a simple linear projection after SiLU activation:

$$X_s = \sigma(\Phi_2(X_1)), \quad (9)$$

Following the design pattern shown in the block diagrams, the outputs from both branches are combined and processed through a final layer normalization and projection:

$$Y = \Phi_3(LN(X_m + X_s)), \quad (10)$$

This dual-branch architecture is implemented in both Local Residual State Space Blocks (L-RSSB) and Hierarchical Residual State Space Blocks (H-RSSB), with the key difference lying in their selective scan mechanisms in the main branch. The L-VSSM employs Local-enhanced Selective Scan for preserving local spatial relationships, while H-VSSM incorporates Hierarchical Selective

Scan to enable hierarchical feature processing through varied sampling patterns.

Algorithm 1 Local-Enhanced SS2D

```

1: Inputs: Feature map  $X \in \mathbb{R}^{H \times W \times C}$ 
2: Hyperparameters: Window size  $(w_h, w_w)$ 
3: Initialize output:  $Y = \mathbf{0} \in \mathbb{R}^{H \times W \times C}$ 
4: Create directional variants:  $X_{dir} = [X, X^T, X^F, (X^T)^F]$ 
5: for  $i = 0$  to 3 do
6:   Partition into windows:  $X_{win}^i = \text{Partition}(X_{dir}^i, w_h, w_w)$ 
7:   Convert to sequence:  $S^i = \text{Flatten}(X_{win}^i)$ 
8:   Process with SSM:  $\hat{S}^i = \text{SSM}_i(S^i)$ 
9:   Restore window structure:  $Y_{win}^i = \text{Reshape}(\hat{S}^i, w_h, w_w)$ 
10:  Apply inverse transform:  $Y^i = \text{Inverse}_i(Y_{win}^i)$ 
11:  Accumulate results:  $Y = Y + Y^i$ 
12: end for
13: Return:  $Y$ 

```

4.2 Local-Enhanced SSM

In the context of flare removal, restoring damaged regions requires effective utilization of local semantic consistency. However, in conventional selective scan sequences, spatially adjacent pixels in the original image may be positioned far apart in the sequence. Due to the inherent distance-decay property of State Space Model[32], this can lead to significant attenuation of local contextual information. The local-scan approach proposed by [11], which processes and concatenates image patches separately, effectively addresses this limitation. Building upon this foundation, we further enhance the mechanism by introducing multi-directional scanning patterns to maximally preserve the spatial structural information of the original image.

Specifically, given a scale-specific feature map $X \in \mathbb{R}^{H \times W \times C}$, we divide it into $M \times N$ non-overlapping windows of size $win_h \times win_w$, where $M = H/win_h$ and $N = W/win_w$. Within each window, pixels are scanned in raster order from left to right and top to bottom, generating local subsequences that maintain neighborhood relationships. These subsequences are then concatenated according to their window positions, forming a complete sequence that preserves both local structure and global arrangement.

To maximize the preservation of inherent spatial structures in the original image, we adopt the approach [24] which processes the feature map from multiple perspectives. Specifically, we can transpose the aforementioned hierarchical sub-images and further apply reverse or non-reverse operations to the transposed or non-transposed local image sequences, thereby obtaining scan sequences from four different directions. These four directional sequences are processed by four separate SSM models with different parameters. Finally, the processed sequences are restored to the original image shape, and these four feature maps are simply added together. The detailed algorithm is presented in Algorithm 1.

This approach ensures that local semantic consistency is effectively preserved during the flare removal process, leading to more accurate restoration of flare-affected regions. Detailed ablation study results are presented in Section 4.1.

4.3 Hierarchical Selective Scan Mechanism

Hierarchical mechanism plays a crucial role in image restoration [20]. Effective flare removal requires both the utilization of local textural details and the comprehension of flare patterns that may manifest across broader spatial contexts. To effectively capture and process these hierarchical features, we propose Hierarchical Selective Scan mechanism at decoding stage.

The foundation of our approach lies in a key property of discrete SSMs: the correlation between two elements in a sequence decreases as their distance increases [32]. Inspired by this property, our Hierarchical Selective Scan mechanism implements different stride sampling patterns during the selective scan process, generating multiple sub-sequences at each scale. In these sub-sequences, pixels that were originally distant in the input image become closer, thereby establishing stronger connections through SSM processing. After the SSM operation, these sub-sequences are reshaped back to the original feature map dimensions, yielding scale-specific feature representations that capture long-range dependencies without resolution loss.

To formalize this Hierarchical Selective Scan mechanism, we define i -th level sub-image \mathcal{S}_{ik} of feature map $\mathcal{F} \in \mathbb{R}^{H \times W \times C}$ as:

$$(\mathcal{S}_{ik})_{h,w} = \begin{cases} \mathcal{F}_{h',w'}, & h' \leq H-1, w' \leq W-1 \\ 0, & \text{else} \end{cases} \quad (11)$$

where the mapped coordinates (h', w') are computed as:

$$h' = h_k + 2^i \cdot h, \quad w' = w_k + 2^i \cdot w, \quad (12)$$

with $h_k, w_k \in \{0, 1, \dots, \lceil H/2^i \rceil - 1\}$ being the top-left coordinate of the k -th sub-image, where $k \in \{0, 1, \dots, 2^i - 1\}$ is the sub-image index and h, w are the spatial coordinates in the sub-image. To facilitate efficient batch processing in our SSM operations, all sub-images are zero-padded to match the dimensions of the largest sub-image.

Each sub-image is then processed by our Local-enhanced SSM module to obtain processed sub-features:

$$\hat{\mathcal{S}}_{ik} = LSSM_i(\mathcal{S}_{ik}), \quad (13)$$

where $LSSM_i$ denotes the Local-enhanced SSM operation at scale level i . These processed sub-features are then reverse-mapped to reconstruct scale-specific features:

$$\tilde{\mathcal{F}}_i = \text{Reverse} \left(\left\{ \hat{\mathcal{S}}_{ik} \right\}_{k=0}^{2^i-1} \right), \quad (14)$$

where Reverse is the function that maps processed sub-images back to the original feature space. Finally, we integrate features across all K scale levels to obtain the enhanced feature representation:

$$\tilde{\mathcal{F}} = \frac{1}{K} \sum_{i=1}^K \tilde{\mathcal{F}}_i, \quad (15)$$

Notably, our approach operates in a divide-and-conquer-like manner on the original feature map, fundamentally differing from previous methods that rely on resolution reduction.

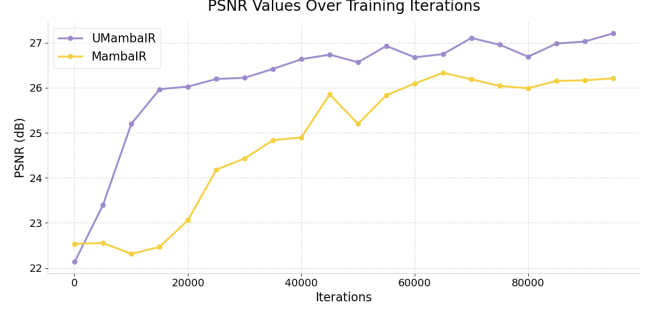


Figure 4: PSNR values over training iterations for U-shaped MambaIR and MambaIR architectures. The U-shaped structure demonstrates faster convergence and better performance compared to the MambaIR.

Table 1: Ablation Study on Local-Enhanced and Hierarchical Components

Model Configuration	PSNR	SSIM
Baseline	27.354	0.894
+ Local-enhanced SS2D	27.627	0.896
+ Hierarchical Selective Scan	27.778	0.899

5 EXPERIMENTS

5.1 Implementation Details

We train our network on the Flare7K++ dataset[5]. For flare synthetic process, we follow the strategy as Flare7K++, where paired flare-corrupted and flare-free images are generated on-the-fly by sampling background images from the 24K Flickr dataset[44]. To enhance the diversity and robustness of the training data, we apply various augmentation techniques including random rotation, translation, shearing, scaling, blurring, and color adjustments. All these data augmentation settings are kept identical to those in Flare7K++ to ensure fair comparison.

Our network training framework and settings are the same as Flare7k++. Specifically, input images are center-cropped to 512×512 , and the model is trained with a batch size of 2 using the Adam [14] optimizer with a learning rate of $1e-4$ for 300k iterations. The backbone outputs six channels, where the first three channels represent the flare-free image and the latter three channels correspond to the flare image. These outputs are used to compute the loss function:

$$\hat{I}_0, \hat{F} = \mathcal{N}(I), \quad (16)$$

$$L(\hat{y}, y) = L_1(\hat{y}, y) + L_{\text{ogg}}(\hat{y}, y), \quad (17)$$

$$L_{\text{rec}} = |I - \text{Clip}(\hat{I}_0 \oplus \hat{F})|, \quad (18)$$

$$L_{\text{total}} = w_1 L(\hat{I}_0, I_0) + w_2 L(\hat{F}, F) + w_3 L_{\text{rec}}, \quad (19)$$

where \mathcal{N} takes the flare-corrupted image I as input and outputs the predicted flare-free image \hat{I}_0 and flare component \hat{F} . Both outputs are compared with their ground truth counterparts (I_0 and F) using loss function L that combines L1 and VGG [33] perceptual losses, while L_{rec} measures the reconstruction error between the input



Figure 5: Qualitative comparison of flare removal results. From left to right: Input image with lens flares, Restormer, Uformer, DeflareMamba (Ours), and Ground Truth (GT). Our method better preserves image details near light sources and achieves cleaner removal of streak artifacts, leading to more visually pleasing results that closely match the ground truth.

Table 2: Quantitative Comparison with State-of-the-art Methods

Metric	Network trained on Flare7K++								
	Input	U-Net[38]	HINet[13]	MPRNet*[26]	Restormer*[41]	Uformer[38]	DiffIare [46]	Kopt.el[15]	DeflareMamba (Ours)
PSNR↑	22.56	27.19	27.55	27.04	27.60	27.63	26.06	27.66	27.78
SSIM↑	0.857	0.894	0.892	0.893	0.897	0.894	0.898	0.897	0.899

image and the recomposed image from predictions. The total loss L_{total} is a weighted combination. We empirically set $w_1 = w_2 = w_3 = 1$, which is consistent with the settings in Flare7K++.

5.2 Ablation Study

Effect of U-shaped Network Architecture. Our framework adopts a U-shaped architecture to gradually expand the receptive field of SSM elements while reducing sequence lengths. For ablation studies on U-shaped architecture, we use MambaIR[10] as the baseline. We then introduce U-shaped MambaIR by incorporating downsampling and upsampling operations into MambaIR. Experiments demonstrate that this design effectively maintains contextual consistency throughout the network.

As shown in Figure 4, U-shaped MambaIR achieves faster convergence compared to the baseline MambaIR[10]. During early training

(first 20k iterations), the U-shaped network gains nearly 3dB advantage. After complete training, it maintains approximately 1dB higher PSNR, confirming that the U-shaped structure effectively addresses SSM limitations.

Effect of Local-Enhanced and Hierarchical Mechanism. As discussed earlier, flare removal tasks require both global perception and local focus for effective restoration. We select the aforementioned U-shaped MambaIR as our baseline. We first replace the standard SS2D in baseline with Local-enhanced SS2D. Then, we further introduce the Hierarchical Selective Scan mechanism to the model. Table 1 presents the quantitative results.

The ablation study demonstrates significant PSNR improvements from our proposed components. The Local-enhanced SS2D improves the baseline PSNR by 0.273dB, indicating its effectiveness in preserving local spatial relationships and fine-grained details. Furthermore, the Hierarchical Selective Scan mechanism adds another

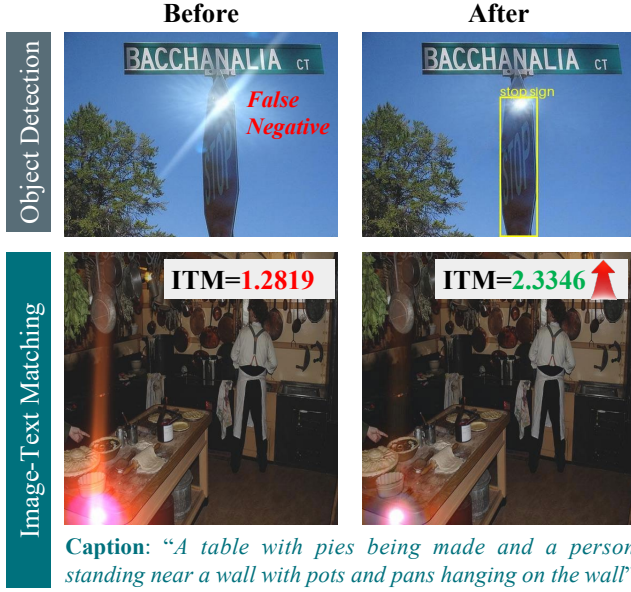


Figure 6: Visual results of object detection and image-text matching before/after flare removal. Our method successfully prevents the false negative detection of the street sign and improves the image-text matching score.

0.151dB gain, confirming its ability to establish stronger long-range dependencies across different scales. Together, these components achieve a total improvement of 0.424dB while maintaining consistent gains in SSIM[37].

5.3 Comparison with SOTAs

To evaluate the effectiveness of our proposed DeflareMamba, we conduct comprehensive comparisons with state-of-the-art networks trained on Flare7K++. For a fair comparison, we evaluate all methods on the same test set and report standard evaluation metrics including PSNR and SSIM[37]. Methods marked with asterisks (*) indicate reduced parameter configurations, with implementation details following Flare7K++ [5].

As shown in Table 2, DeflareMamba achieves the best performance among all compared methods. Specifically, it outperforms the previous best performer Uformer[38] by 0.145dB in PSNR. For SSIM [37], our method achieves 0.899, which is 0.005 higher than Uformer (0.894) and 0.002 better than the previous best performer Restormer [41](0.897). These improvements demonstrate the effectiveness of our approach in preserving both structural and perceptual image quality. Visual comparisons in Figure 5 further reveal that our method restores more distorted details and reduces flare artifacts more completely. More implementation details and comparison results are available in supplementary materials.

5.4 Performance on Downstream Tasks

To evaluate our method’s impact on downstream tasks, we synthesize test images by applying flare effects from Flare7K++ to the COCO [23] validation set. We then compare the performance of

Table 3: Object Detection Performance (mAP)

Data	Faster R-CNN [7]	Deform. DETR [49]	YOLO8x [35]
w/ flare	28.15	36.20	38.15
Uformer	29.13	37.35	39.04
DeflareMamba	29.35	37.59	39.36

Table 4: Vision-Language Alignment Performance

Data	CLIP[29]	BLIP[18]			
	CS	CS	ITM	TR@1	TR@5
w/ flare	28.57	45.31	117.56	72.2	90.1
Uformer	29.14	46.37	127.79	73.1	91.0
DeflareMamba	29.22	46.50	128.45	73.4	91.5

pre-trained models on these flare-corrupted images before and after processing with Uformer [38] and our DeflareMamba.

We evaluate our method using pre-trained models for object detection and vision-language alignment tasks on the COCO dataset. For object detection, we measure the mean Average Precision (mAP). For vision-language alignment, we assess both the semantic alignment quality through similarity scores and text-to-image retrieval performance using Top-k recall rates (TR@k). As shown in Table 3 and Table 4, our method consistently outperforms both flare-corrupted inputs and Uformer across all metrics, demonstrating its effectiveness in preserving semantic information for downstream tasks. More details are provided in the supplementary materials.

6 CONCLUSION AND DISCUSSION

In this paper, we propose DeflareMamba, the first Mamba-based architecture for flare removal that effectively maintains global-local contextual consistency. We adopt a U-shaped architecture to mitigate the long-term decay issue in SSMs by reducing sequence lengths while aggregating neighboring pixel information. To better preserve local semantic consistency, we employ the Local-enhanced SS2D mechanism with multi-directional scanning patterns. Moreover, we propose a novel Hierarchical Selective Scan mechanism that captures hierarchical contextual information through cross-level pixel sampling. Extensive experiments demonstrate that our method not only outperforms state-of-the-art flare removal approaches but also enhances both object detection performance and vision-language semantic understanding by reducing flare-induced information distortion.

Discussion. While our method demonstrates significant improvements in flare removal, there are several directions for future research. First, the complete removal of long streak artifacts in scattering flares remains challenging, suggesting the need for improved architectures or data augmentation strategies. Second, our current single-block hierarchical feature processing could be distributed across multiple blocks while maintaining the total block count, potentially reducing computational complexity.

ACKNOWLEDGMENTS

This work was supported in part by the National Natural Science Foundation of China under Grant 62202056, and the Fundamental Research Funds for the Central Universities under Grant 2243100002.

REFERENCES

- [1] CS Asha, Sooraj Kumar Bhat, Deepa Nayak, and Chaithra Bhat. 2019. Auto removal of bright spot from images captured against flashing light source. In *2019 IEEE International Conference on Distributed Computing, VLSI, Electrical Circuits and Robotics (DISCOVER)*. IEEE, 1–6.
- [2] Floris Chabert. 2015. Automated lens flare removal. In *Technical report*. Department of Electrical Engineering, Stanford University.
- [3] A. Criminisi, P. Perez, and K. Toyama. 2004. Region filling and object removal by exemplar-based image inpainting. *IEEE Transactions on Image Processing* 13, 9 (2004), 1200–1212.
- [4] Yuekun Dai, Chongyi Li, Shangchen Zhou, Ruicheng Feng, and Chen Change Loy. 2022. Flare7k: A phenomenological nighttime flare removal dataset. *Advances in Neural Information Processing Systems* 35 (2022), 3926–3937.
- [5] Yuekun Dai, Chongyi Li, Shangchen Zhou, Ruicheng Feng, Yihang Luo, and Chen Change Loy. 2024. Flare7k+: Mixing Synthetic and Real Datasets for Nighttime Flare Removal and Beyond. *IEEE Transactions on Pattern Analysis and Machine Intelligence* 46, 11 (2024), 7041–7055.
- [6] Chao Dong, Chen Change Loy, Kaiming He, and Xiaoou Tang. 2014. Learning a deep convolutional network for image super-resolution. In *Computer Vision–ECCV 2014: 13th European Conference, Zurich, Switzerland, September 6–12, 2014, Proceedings, Part IV 13*. Springer, 184–199.
- [7] Ross Girshick. 2015. Fast r-cnn. In *Proceedings of the IEEE international conference on computer vision*. 1440–1448.
- [8] Albert Gu and Tri Dao. 2023. Mamba: Linear-time sequence modeling with selective state spaces. *arXiv preprint arXiv:2312.00752* (2023).
- [9] Albert Gu, Karan Goel, and Christopher Ré. 2022. Efficiently Modeling Long Sequences with Structured State Spaces. In *The International Conference on Learning Representations (ICLR)*.
- [10] Hang Guo, Jinmin Li, Tao Dai, Zhihao Ouyang, Xudong Ren, and Shu-Tao Xia. 2024. Mambair: A simple baseline for image restoration with state-space model. In *European conference on computer vision*. Springer, 222–241.
- [11] Tao Huang, Xiaohuan Pei, Shan You, Fei Wang, Chen Qian, and Chang Xu. 2024. Localmamba: Visual state space model with windowed selective scan. *arXiv preprint arXiv:2403.09338* (2024).
- [12] Matthias Hullin, Elmar Eisemann, Hans-Peter Seidel, and Sungkil Lee. 2011. Physically-based real-time lens flare rendering. In *ACM SIGGRAPH 2011 papers*. 1–10.
- [13] Junpeng Jing, Xin Deng, Mai Xu, Jianyi Wang, and Zhenyu Guan. 2021. Hinet: Deep image hiding by invertible network. In *Proceedings of the IEEE/CVF international conference on computer vision*. 4733–4742.
- [14] Diederik P. Kingma and Jimmy Ba. 2015. Adam: A Method for Stochastic Optimization. In *3rd International Conference on Learning Representations, ICLR 2015, San Diego, CA, USA, May 7–9, 2015, Conference Track Proceedings*, Yoshua Bengio and Yann LeCun (Eds.).
- [15] Yousef Kotb and Marwan Torki. 2024. Flare-Free Vision: Empowering Uformer with Depth Insights. In *ICASSP 2024 - 2024 IEEE International Conference on Acoustics, Speech and Signal Processing (ICASSP)*. 2565–2569. <https://doi.org/10.1109/ICASSP48485.2024.10446006>
- [16] Fengbo Lan and Chang Wen Chen. 2024. Understanding and Tackling Scattering and Reflective Flare for Mobile Camera Systems. In *Proceedings of the 32nd ACM International Conference on Multimedia*. 8768–8776.
- [17] Dawa Chyophel Lepcha, Bhawna Goyal, Ayush Dogra, and Vishal Goyal. 2023. Image super-resolution: A comprehensive review, recent trends, challenges and applications. *Information Fusion* 91 (2023), 230–260.
- [18] Junnan Li, Dongxu Li, Caiming Xiong, and Steven Hoi. 2022. Blip: Bootstrapping language-image pre-training for unified vision-language understanding and generation. In *International conference on machine learning*. PMLR, 12888–12900.
- [19] Xiaoyu Li, Bo Zhang, Jing Liao, and Pedro V Sander. 2021. Let's see clearly: Contaminant artifact removal for moving cameras. In *Proceedings of the IEEE/CVF International Conference on Computer Vision*. 2011–2020.
- [20] Yawei Li, Yuchen Fan, Xiaoyu Xiang, Denis Demandolx, Rakesh Ranjan, Radu Timofte, and Luc Van Gool. 2023. Efficient and explicit modelling of image hierarchies for image restoration. In *Proceedings of the IEEE/CVF Conference on Computer Vision and Pattern Recognition*. 18278–18289.
- [21] Jingyun Liang, Jiezhang Cao, Guolei Sun, Kai Zhang, Luc Van Gool, and Radu Timofte. 2021. Swinir: Image restoration using swin transformer. In *Proceedings of the IEEE/CVF international conference on computer vision*. 1833–1844.
- [22] Bee Lim, Sanghyun Son, Heewon Kim, Seungjun Nah, and Kyoung Mu Lee. 2017. Enhanced deep residual networks for single image super-resolution. In *Proceedings of the IEEE conference on computer vision and pattern recognition workshops*. 136–144.
- [23] Tsung-Yi Lin, Michael Maire, Serge Belongie, James Hays, Pietro Perona, Deva Ramanan, Piotr Dollár, and C Lawrence Zitnick. 2014. Microsoft coco: Common objects in context. In *Computer vision–ECCV 2014: 13th European conference, zurich, Switzerland, September 6–12, 2014, proceedings, part v 13*. Springer, 740–755.
- [24] Yue Liu, Yunjie Tian, Yuzhong Zhao, Hongtian Yu, Lingxi Xie, Yaowei Wang, Qixiang Ye, Jianbin Jiao, and Yunfan Liu. 2024. Vmamba: Visual state space model. *Advances in neural information processing systems* 37 (2024), 103031–103063.
- [25] Ze Liu, Yutong Lin, Yue Cao, Han Hu, Yixuan Wei, Zheng Zhang, Stephen Lin, and Baining Guo. 2021. Swin transformer: Hierarchical vision transformer using shifted windows. In *Proceedings of the IEEE/CVF international conference on computer vision*. 10012–10022.
- [26] Armin Mehri, Parichehr B Ardakani, and Angel D Sappa. 2021. MPRNet: Multi-path residual network for lightweight image super resolution. In *Proceedings of the IEEE/CVF Winter Conference on Applications of Computer Vision*. 2704–2713.
- [27] Andreas Nussberger, Helmut Grabner, and Luc Van Gool. 2015. Robust aerial object tracking in images with lens flare. In *2015 IEEE International Conference on Robotics and Automation (ICRA)*. IEEE, 6380–6387.
- [28] Xiaohuan Pei, Tao Huang, and Chang Xu. 2024. EfficientVMamba: Atrous Selective Scan for Light Weight Visual Mamba. *arXiv preprint arXiv:2403.09977* (2024).
- [29] Alec Radford, Jong Wook Kim, Chris Hallacy, Aditya Ramesh, Gabriel Goh, Sandhini Agarwal, Girish Sastry, Amanda Askell, Pamela Mishkin, Jack Clark, et al. 2021. Learning transferable visual models from natural language supervision. In *International conference on machine learning*. PMLR, 8748–8763.
- [30] Dikpal Reddy and Ashok Veeraraghavan. 2021. Lens flare and lens glare. In *Computer Vision: A Reference Guide*. Springer, 741–744.
- [31] Olaf Ronneberger, Philipp Fischer, and Thomas Brox. 2015. U-net: Convolutional networks for biomedical image segmentation. In *Medical image computing and computer-assisted intervention–MICCAI 2015: 18th international conference, Munich, Germany, October 5–9, 2015, proceedings, part III 18*. Springer, 234–241.
- [32] Yuheng Shi, Mingjing Dong, and Chang Xu. 2024. Multi-scale vmamba: Hierarchy in hierarchy visual state space model. *Advances in Neural Information Processing Systems*.
- [33] Karen Simonyan and Andrew Zisserman. 2015. Very deep convolutional networks for large-scale image recognition. *International Conference on Learning Representation*.
- [34] Soonyong Song and Heechul Bae. 2023. Hard-negative sampling with cascaded fine-tuning network to boost flare removal performance in the nighttime images. In *Proceedings of the IEEE/CVF Conference on Computer Vision and Pattern Recognition*. 2843–2852.
- [35] Rejin Varghese and Sambath M. 2024. YOLOv8: A Novel Object Detection Algorithm with Enhanced Performance and Robustness. In *2024 International Conference on Advances in Data Engineering and Intelligent Computing Systems (ADICS)*. 1–6.
- [36] Patricia Vitoria and Coloma Ballester. 2019. Automatic flare spot artifact detection and removal in photographs. *Journal of Mathematical Imaging and Vision* 61, 4 (2019), 515–533.
- [37] Zhou Wang, Alan C Bovik, Hamid R Sheikh, and Eero P Simoncelli. 2004. Image quality assessment: from error visibility to structural similarity. *IEEE transactions on image processing* 13, 4 (2004), 600–612.
- [38] Zhendong Wang, Xiaodong Cun, Jianmin Bao, Wengang Zhou, Jianzhuang Liu, and Houqiang Li. 2022. Uformer: A general u-shaped transformer for image restoration. In *Proceedings of the IEEE/CVF conference on computer vision and pattern recognition*. 17683–17693.
- [39] Yicheng Wu, Qiurui He, Tianfan Xue, Rahul Garg, Jiawen Chen, Ashok Veeraraghavan, and Jonathan T Barron. 2021. How to train neural networks for flare removal. In *Proceedings of the IEEE/CVF International Conference on Computer Vision*. 2239–2247.
- [40] Chenhongyi Yang, Zehui Chen, Miguel Espinosa, Linus Ericsson, Zhenyu Wang, Jiaming Liu, and Elliot J. Crowley. 2024. PlainMamba: Improving Non-Hierarchical Mamba in Visual Recognition. In *35th British Machine Vision Conference 2024, BMVC 2024, Glasgow, UK, November 25–28, 2024*. BMVA.
- [41] Syed Waqas Zamir, Aditya Arora, Salman Khan, Munawar Hayat, Fahad Shahbaz Khan, and Ming-Hsuan Yang. 2022. Restormer: Efficient transformer for high-resolution image restoration. In *Proceedings of the IEEE/CVF conference on computer vision and pattern recognition*. 5728–5739.
- [42] Syed Waqas Zamir, Aditya Arora, Salman Khan, Munawar Hayat, Fahad Shahbaz Khan, Ming-Hsuan Yang, and Ling Shao. 2021. Multi-stage progressive image restoration. In *Proceedings of the IEEE/CVF conference on computer vision and pattern recognition*. 14821–14831.
- [43] Dafeng Zhang, Jia Ouyang, Guanqun Liu, Xiaobing Wang, Xiangyu Kong, and Zhehu Jin. 2023. FF-former: Swin fourier transformer for nighttime flare removal. In *Proceedings of the IEEE/CVF conference on computer vision and pattern recognition*. 2824–2832.

- [44] Xuaner Zhang, Ren Ng, and Qifeng Chen. 2018. Single image reflection separation with perceptual losses. In *Proceedings of the IEEE conference on computer vision and pattern recognition*. 4786–4794.
- [45] Yulun Zhang, Kunpeng Li, Kai Li, Lichen Wang, Bineng Zhong, and Yun Fu. 2018. Image super-resolution using very deep residual channel attention networks. In *Proceedings of the European conference on computer vision (ECCV)*. 286–301.
- [46] Tianwen Zhou, Qihao Duan, and Zitong YU. 2024. DiffLare: Removing Image Lens Flare with Latent Diffusion Models. In *35th British Machine Vision Conference 2024, BMVC 2024, Glasgow, UK, November 25-28, 2024*. BMVA. <https://papers.bmvc2024.org/0437.pdf>
- [47] Yuyan Zhou, Dong Liang, Songcan Chen, Sheng-Jun Huang, Shuo Yang, and Chongyi Li. 2023. Improving lens flare removal with general-purpose pipeline and multiple light sources recovery. In *Proceedings of the IEEE/CVF international conference on computer vision*. 12969–12979.
- [48] Lianghui Zhu, Bencheng Liao, Qian Zhang, Xinlong Wang, Wenyu Liu, and Xinggang Wang. 2024. Vision Mamba: Efficient Visual Representation Learning with Bidirectional State Space Model.
- [49] Xizhou Zhu, Weijie Su, Lewei Lu, Bin Li, Xiaogang Wang, and Jifeng Dai. 2021. Deformable detr: Deformable transformers for end-to-end object detection. *International Conference on Learning Representation*.